

## Electron energy-loss spectroscopy of electron states in isolated carbon nanostructures

K. Suenaga,<sup>1,2,\*</sup> E. Sandré,<sup>1</sup> C. Colliex,<sup>1,3</sup> C. J. Pickard,<sup>4</sup> H. Kataura,<sup>5</sup> and S. Iijima<sup>2</sup>

<sup>1</sup>Laboratoire de Physique des Solides, UMR CNRS 8502, Building 510, Université Paris-Sud, Orsay 91405, France

<sup>2</sup>Japan Science and Technology Corporation, Meijo University, Nagoya 468-8502, Japan

<sup>3</sup>Laboratoire Aimé Cotton, UPR CNRS 3321, Building 505, Université Paris-Sud, Orsay 91405, France

<sup>4</sup>Institut für Geowissenschaften, Kristallographie/Mineralogie, Olshausenstrasse 40, Kiel D-24098, Germany

<sup>5</sup>Department of Physics, Tokyo Metropolitan University, Tokyo 192-0397, Japan

(Received 22 September 2000; published 3 April 2001)

Electronic states of an isolated nano-object made of single graphene layer have been successfully explored by means of electron energy-loss spectroscopy with high sensitivity and high spatial resolution. In further systematic study of various carbon nanostructures, the curvature and/or the interlayer coupling between adjacent graphene layers have been proved to govern the electronic states of carbon nanostructures. Using density functional theory, experimentally observed variations of the carbon  $K$  ( $1s$ ) near-edge fine structure have been ascribed mostly to the increasing curvature of the graphene layers.

DOI: 10.1103/PhysRevB.63.165408

PACS number(s): 73.22.-f, 71.15.Mb, 81.05.Tp, 82.80.Pv

The knowledge of the distribution of electron states in isolated quantum object is of prime importance as they govern their electronic properties. The family of carbon nanostructures has grown steadily over the past decade, with the discovery of variable morphologies and diversified physical properties.<sup>1</sup> Graphene layers (two-dimensional hexagonal networks of  $sp^2$  carbon) have so far been reported with different shapes and interactions: multiwalled or single-walled carbon layers in tubular, horn-shaped, or spherical geometry, so-called nanotubes (MWNT or SWNT), nanohorns and nano-onions, respectively. And several types of aggregates made of these elementary components (i.e., nanotubulites) have very recently been identified, using high-resolution transmission electron microscopy (HRTEM) techniques.<sup>2,3</sup> The electron states (both occupied and vacant states) of these carbon nano-objects have been predicted to vary with the coupling and/or curvature of the graphene layers.<sup>4,5</sup> In this context, it is important to experimentally investigate the electronic states in well-characterized carbon nano-objects.

Electron energy-loss spectroscopy (EELS), performable within a TEM, probes the unoccupied electron states over a wide energy range above the Fermi level.<sup>6</sup> In the small-angle experimental conditions, the information obtained is similar to the one provided by x-ray absorption technique. However, as the TEM is able to visualize and select single nano-objects with well-defined dimension, shape, and stacking of layers, the spectral and morphological information can be exactly connected at the subnanometer level.<sup>7</sup> In this paper, we compare experimental EELS spectra acquired from well-defined carbon nano-objects with results of *ab initio* electronic structure calculations that have been performed for model structures containing the correct number of carbon atoms to reproduce the relevant changes in stacking and curvature.

A collection of carbon nano-objects made of single graphene layers with a variety of morphologies has been prepared using various techniques. Tubular or horn-shaped closed graphene structures with different inner diameters, inter-layer couplings, and/or different curvatures were prepared by a  $\text{CO}_2$  laser ablation method.<sup>3</sup> Double-layered nanotubes, in which the inner nanotube has an extremely

small diameter ( $\sim 0.7$  nm), were obtained by coalescence of  $\text{C}_{70}$  molecules under the 200 kV electron beam<sup>8</sup> within the 1.5-nm-diameter outer tubes selectively produced in a Nd-YAG (yttrium aluminum garnet) laser ablation method by controlling the furnace temperature and the catalyst.<sup>9</sup>

The spatially resolved EELS measurements have been performed with a dedicated scanning TEM (STEM, VG-HB501). The incident electron beam (100 kV) was focused into a probe of about 0.5 nm diameter. For each probe position, successively addressed with 0.3-nm step, the EELS spectrum was recorded with a parallel detector (Gatan PEELS 666).<sup>10</sup> Such a collection of carbon  $K$ -edge spectra, recorded across a nanohorn of  $\sim 3$  nm dimension is shown in Fig. 1. For each spectrum the acquisition time was reduced to 0.5 sec in order to prevent electron irradiation damage. Under such conditions, the jump ratio for the spectrum goes up to several hundred counts at the C  $K$ -edge onset (285 eV) and allows the fine structure analysis with sufficiently good statistics.

The carbon profile (i.e., the integrated C  $K$  signal over a given energy window, after background subtraction) across the nanohorn is shown in Fig. 1(a), together with an annular dark field (ADF) profile that was simultaneously recorded. Both profiles exhibit two peaks with a hollow center, which is characteristic of an empty cylindrical object. The present results clearly demonstrate that chemical profiling and fine structure analysis based on spatially resolved EELS are possible on a *single graphene layer* of carbon, in which only a few tens of carbon atoms contribute to each spectrum.

Figure 2 gathers high-resolution micrographs and accompanying schematic representations for various morphologies of interacting graphene layers. Figure 2(a) shows well-stacked graphene layers (10 layers) in a cylindrical configuration with a 10–16 nm diameter (in a cross-sectional view). The layers are coupled in such a graphitized MWNT. Figure 2(b) shows an aggregate of nanohorns of 3 nm diameter.<sup>3</sup> The coupled double-layer configuration is dominant in this aggregate. Such coupling of adjacent layers does not exist in bundles of SWNT's with smaller diameter ( $\sim 1.5$  nm), because the elastic force acting on each graphene layer to keep

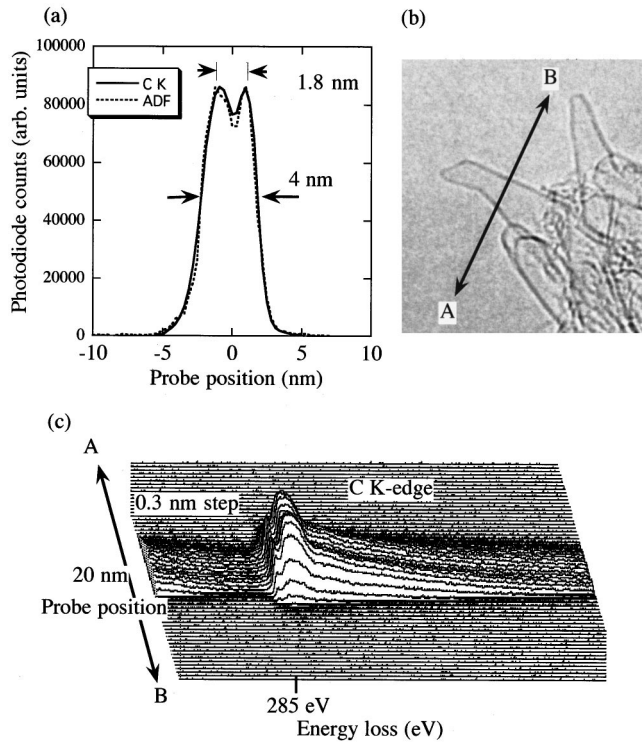


FIG. 1. (a) The C *K*-edge and ADF counts extracted from the line spectrum recorded when the incident probe is scanned across a similar nanohorn to that shown in the bright-field image (b) (from point A to B). (c) A perspective view of the acquired 64 EELS spectra on the C *K*-edge recorded with steps of 0.3 nm. The  $\pi^*$  peak (unlike that of amorphous or damaged carbon) is clearly seen and the  $\sigma^*$  fine structure is more rounded compared to that of graphite.

the nanotubes in cylindrical shape largely overcomes the van der Waals force between the adjacent graphene layers when the diameter of the nanotube is small enough.<sup>11</sup> Figure 2(c) displays another type of clustering of elongated fullerenes with various sizes and shapes.<sup>3</sup> The diameters of these fullerenes cover a wide range of distances between 1 and 3 nm. Figure 2(d) is a cross-sectional view of double-layered nanotubes with well-controlled diameters, 0.7 nm for the inner tubes and 1.5 nm for the outer ones. The smallest diameter for the stable SWNT's is 0.7 nm. Consequently these present the highest curvature that can be expected for accessible nanotubes. As the nanohorn consists of a single graphene layer that is free of adjacent layers, it offers an appropriate spectrum for a (nearly) free-standing single atomic layer of carbon; see Fig. 2(e).

Curves I–V in Fig. 3 gather the EELS carbon *K* ( $1s$ ) near-edge structures, which have been recorded for the morphologies illustrated in Fig. 2. In all cases the electron beam propagates parallelly by or tangentially to the graphene layers plane. It gives rise to scattering events incorporating momentum transfer parallel as well as perpendicular to the local *c* axis of the layered structure. Together with the values of the angles of illumination and collection used (respectively, 7.5 and 22 mrad), these experimental conditions tend to average anisotropy effects. The sharp peak (marked *a*) at  $\sim 285$

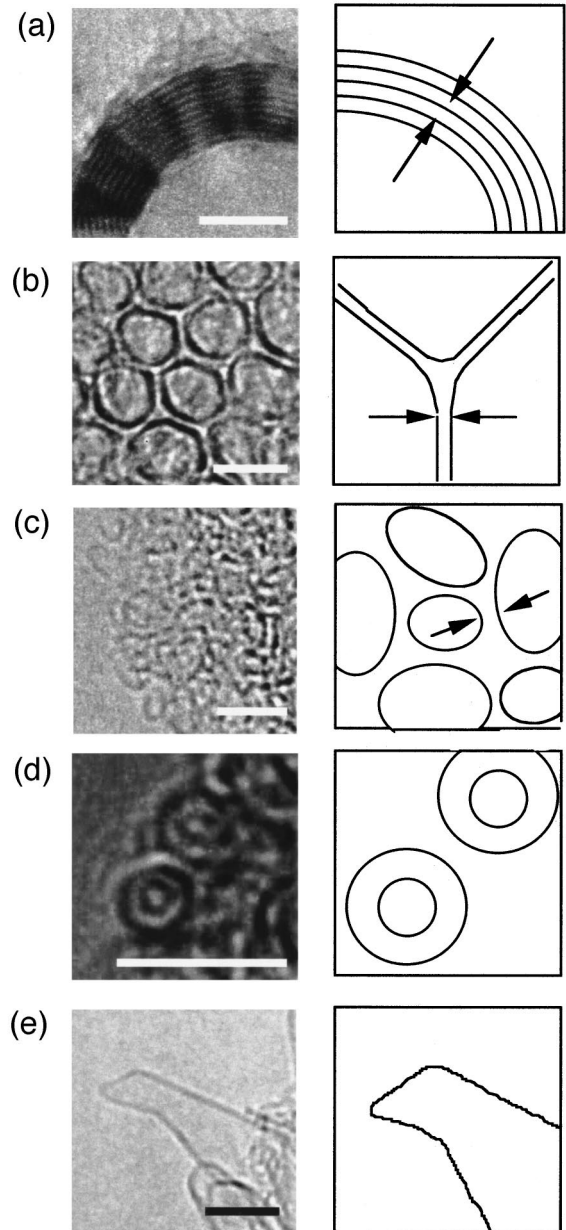


FIG. 2. High-resolution images displaying various morphologies of graphene layers in carbon nano-objects (Bar=3 nm). (a) a MWNT consisting of well-stacked graphitized layers (in cross view) of 10–16 nm diameter. (b) Coupled double-layers in an aggregate of nanohorns of  $\sim 3$  nm diameter. (c) An aggregate of various sized fullerenes (1–3 nm), in which the adjacent fullerenes are decoupled with weaker interlayer interaction. (d) Double-walled carbon nanotubes with well-controlled diameters (0.7 nm for inner tube and 1.5 nm for outer tube). (e) An isolated nanohorn consisting of a curved free-standing single graphene layer with no adjacent layer. Accompanying illustrations for each image are not drawn in the same scale. The decreasing diameter accounts for the increasing curvature.

eV is due to the transition from  $1s$  to  $\pi^*$ , while the four peaks (*b*–*e*) correspond to the  $\sigma^*$  region (290–310 eV). There is a systematic evolution in the edge structures of the spectra (I–IV) as the curvature radius (*R*) of the examined

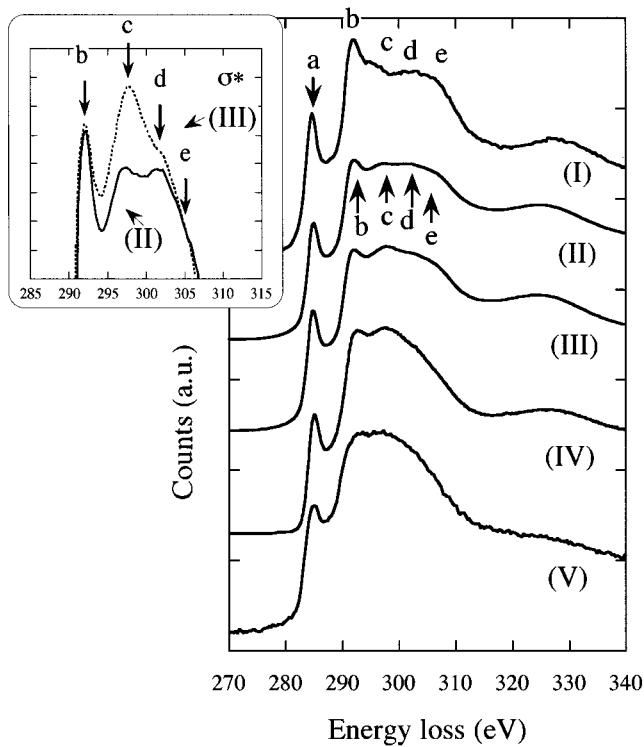


FIG. 3. (I–V) A series of C  $K$ -edge fine structures corresponding to the various carbon nano-objects shown in Figs. 2(a)–2(e), respectively.

nano-objects decreases: (i) the intensity of peak  $b$  decreases, (ii) the peak  $c$  shifts to higher energy, and (iii) the peaks  $c$ ,  $d$ , and  $e$  merge together and grow wider. The subtle changes in the  $\sigma^*$  region are emphasized in the inset figure for the spectra (II) and (III). If the curvature effect dominates the near-edge structure of the graphene sheet, the spectrum (V) for the isolated nanohorn of about 3 nm diameter should be similar to spectrum (II) with rather equivalent curvature. However, the spectrum (V) indeed shows a distinct behavior with smoother shapes in both the  $\pi^*$  and  $\sigma^*$  regions from the spectrum (II) or (III). This may result from the fact that the isolated single graphene layer in the protruding nanohorn is less stable than the coupled ones and can be affected under the incident electron beam with high current flux.

A series of EELS spectrum simulations based on *ab initio* plane-wave electronic structure calculations<sup>12</sup> has been performed in order to understand more quantitatively the differences in the EELS spectra recorded for the different structures. The method we have used is extensively described in Refs. 13 and 14 and has proved to be very efficient in estimating the position of the different peaks in EELS spectra of different carbon structures. Our simulations are based on several approximations: we have supposed the dipolar approximation to estimate the electronic transition strength between the  $1s$  orbital of the carbon atoms and the empty states above the Fermi level; whatever the excitation energy, we have considered that the excited states had infinite lifetime, which implies that we overestimate the intensities of high-energy peaks; and finally we have considered that the electronic structure is not perturbed by the excitation of one core

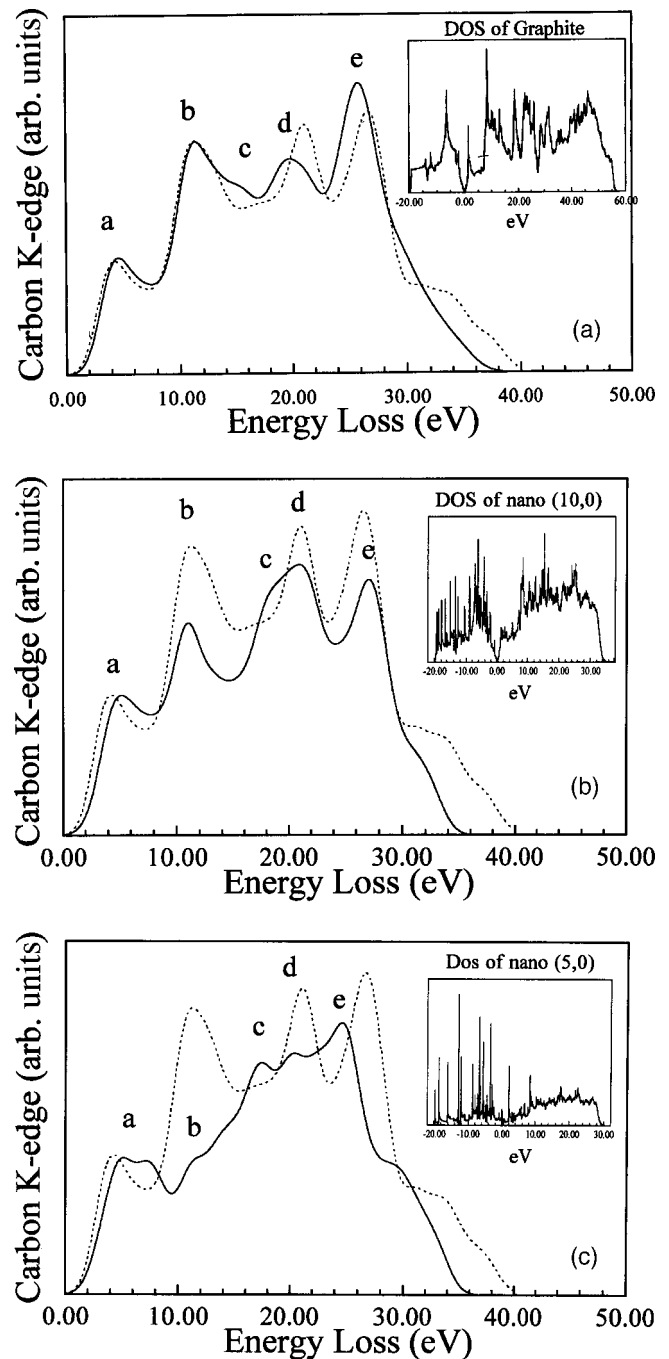


FIG. 4. (a)–(c) The calculated EELS spectra for graphene ( $R = \infty$ ), (10, 0) nanotubes ( $R \sim 0.4$  nm) and (5, 0) nanotubes ( $R \sim 0.2$  nm). The dashed line in each figure represents one for the planar graphite. Inset is the calculated total density of states for each.

electron ( $1s$ ) and that the empty states correspond to those of the unperturbed structure (no core-hole effect is included).

Figures 4(a)–4(c) show the simulated EELS carbon  $K$  edges considering three different structures, namely, (a) planar *single* graphene layer, (b) nanotube with a 0.8 nm diameter ( $R \sim 0.4$  nm), and (c) nanotube with a 0.4 nm diameter ( $R \sim 0.2$  nm). In Fig. 4(a), we show the spectral differences when exciting the planar *single* graphene layer (plain line) compared to the well-stacked planar graphite (dashed line).

Actually no drastic changes between the single graphene and perfect graphite are seen except for slight energy displacements of the *c*, *d*, and *e* peaks. This is not surprising because the involved  $\sigma^*$  states are not sensitive to interlayer interaction as long as they remain of van-der-Waals-type coupling. It further confirms that changes in the EELS spectrum for the spectrum (V) in Fig. 3 should not be attributed to the noninteracting character of the single graphene layer but more reasonably to its sensitivity (vibration, modification) under the beam.

Figures 4(b) and 4(c) represent the calculated EELS spectra for the (10, 0) and (5, 0) crystalline nanoropes, built out of a two-dimensional hexagonal lattice of (10, 0) and (5, 0) nanotubes, respectively,<sup>15</sup> as a model of graphene layer with a constant curvature ( $R=0.4$  and  $0.2$  nm). The latter corresponds to an extremely curved structure that has not yet been observed experimentally as an isolated object. Comparing these calculated spectra to the graphite one should help in understanding the effect of curvature on the experimental EELS spectra. When considering the highly curved (5, 0) nanotubes, one should expect the  $\pi^*$  peak to be doubled because the bonds along the tube direction and the bonds along the circumference become quite different. Obviously, no such high curvatures corresponding to the typical  $R$  value of the order of 0.2 nm seem to be present in our samples. This  $\pi^*$  doubling is not observed in the simulated spectrum for the (10, 0) nanotubes but there is a slight broadening of the  $\pi^*$  peak due to its smaller curvature ( $R=0.4$  nm).

Now considering the  $\sigma^*$  edge (peak *b*), one should notice that it disappears as the curvature grows. In the (10, 0) nanotube, its intensity is divided by 1.5, and in the (5, 0) nanotube it has completely disappeared. The intensity of the *b* peak is then a probe of the degree of curvature of the observed graphite layers. This result agrees with the experimental comparison between the increasing curvature ( $1/R$ ) observed in Fig. 2 and the continuous decrease in the intensity of the *b* peak which is found in the EELS spectra in Fig. 3. Comparing the evolution of the *c*, *d*, and *e* peaks in Fig. 4 shows that these three peaks have a tendency to gather around peak *d* as the curvature increases. As shown in Fig. 3, the experimen-

tally observed evolution with curvature of these three peaks is also to coalesce into one single large peak. However, considering spectrum (IV) in Fig. 3, this coalescence process seems to happen more rapidly experimentally than predicted theoretically. Indeed, the coalescence is observed only in the (5, 0) nanotube calculated spectrum together with the total disappearance of peak *b*. This discrepancy between the experimental and simulated spectra may be related to dynamical effects that can blur the substructures in the high-energy  $\sigma^*$  region of the experimental EELS spectrum. It is reasonably understood that the isolated layers or decoupled double layers are more sensitive to the incident electron beam than the firmly coupled layers in terms of vibration or modification under the beam.

In conclusion, we have performed high-resolution EELS measurements on different samples of carbon nanostructures. Since the interlayer interaction has little effect on the electronic structure of unoccupied states, comparing TEM images, EELS spectra, and *ab initio* calculations, we have correlated the systematic variations in the EELS spectra to the curvature of the graphene layers. In practice, we find that for tubulites with diameter greater than 0.8 nm, only moderate changes in the  $\pi^*$  peak should be observed. In the  $\sigma^*$  region, the threshold peak *b* decreases with increasing curvature of the layers and can represent the degree of curvature. Also the higher-energy peaks (*b*, *c*, and *d*) in the  $\sigma^*$ -region shift and merge together with the increasing curvature. However, this, the experimentally observed coalescence of these high-energy peaks would imply much greater curvature than the observed one according to our calculation and therefore may not be attributed to static curvature effects only. To explain this phenomenon and also the degradation of the  $\pi^*$  peak in isolated single sheets, dynamical effects, including radiation damage, should be evoked.

This work was partially supported by an ICORP program ‘‘Nanotubulites’’ established between the JST and the CNRS. H.K. acknowledges the Grant-in-Aid for Scientific Research on the Priority Area ‘‘Fullerenes and Nanotubes’’ by the Ministry of Education, Science, and Culture of Japan.

\*Corresponding author. Email address: suenaga@meijo-u.ac.jp

<sup>1</sup>For example, R. Saito, G. Dresselhaus, and M. S. Dresselhaus, *Physical Properties of Carbon Nanotubes* (Imperial College Press, London, 1998).

<sup>2</sup>A. Thess, R. Lee, P. Nikolaev, H. Dai, P. Petit, J. Robert, C. Xu, Y. H. Lee, S. G. Kim, A. G. Rinzler, D. T. Colbert, G. E. Scuseria, D. Tomanek, J. E. Fischer, and R. E. Smalley, *Science* **273**, 483 (1996).

<sup>3</sup>S. Iijima, M. Yudasaka, T. Yamada, S. Bandow, K. Suenaga, F. Kokai, and K. Takahashi, *Chem. Phys. Lett.* **309**, 165 (2000).

<sup>4</sup>Y.-K. Kwon, S. Saito, and D. Tomanek, *Phys. Rev. B* **58**, R13 314 (1998).

<sup>5</sup>P. E. Lammert, P. Zhang, and V. H. Crespi, *Phys. Rev. Lett.* **84**, 2453 (2000).

<sup>6</sup>C. Colliex, *Advances in Optical and Electron Microscopy* (Academic, London, 1984), Vol. 9, pp. 65–177.

<sup>7</sup>C. Colliex, D. Imhoff, J. A. Perez-Omil, O. Stéphan, K. Suenaga,

and M. Tencé, *J. Electron Microsc.* **48**, 995 (2000).

<sup>8</sup>J. Sloan, R. E. Dunin-Borkowski, J. L. Hutchison, K. S. Coleman, V. Clifford Williams, J. B. Claridge, A. P. E. York, C. Xu, S. R. Bailey, G. Brown, S. Friedrichs, and M. L. H. Green, *Chem. Phys. Lett.* **316**, 191 (2000).

<sup>9</sup>H. Kataura, Y. Kumazawa, Y. Maniwa, Y. Ohtsuka, R. Sen, S. Suzuki, and Y. Achiba, *Carbon* **38**, 1691 (2000).

<sup>10</sup>C. Jeanguillaume and C. Colliex, *Ultramicroscopy* **28**, 252 (1989).

<sup>11</sup>J. Tersoff and R. S. Ruoff, *Phys. Rev. B* **73**, 676 (1994).

<sup>12</sup>M. C. Payne, M. P. Teter, D. C. Allan, T. A. Arias, and J. D. Joannopoulos, *Rev. Mod. Phys.* **64**, 1045 (1992).

<sup>13</sup>C. J. Pickard and M. C. Payne, in *Electron Microscopy and Analysis 1997*, edited by J. M. Rodenburg, Institute of Condensed Matter Series No. 53 (IOP, Bristol, England, 1997), p. 179.

<sup>14</sup>C. J. Pickard and M. C. Payne, *Phys. Rev. B* **59**, 4685 (1999).

<sup>15</sup>For the chiral index of nanotube, see Ref. 1.